Article

One-Pot Preparation of Benzotriazole-Modified Porous Silica for Durable UVA Absorption Ability

Xiaoyan Sun,* Ke Wang, Hailu Liu, Yang Zhao, Yuan Li, and Dong Xie*

Read Online

ACCESS | Metrics & More | Article Recommendations

ABSTRACT: The durable application of poly(butylene adipate-*co*-terephthalate) (PBAT) under atmospheric conditions is restricted by its poor ultraviolet (UV) stability. To improve the anti-aging capacity to UV radiation of the PBAT film, we describe a straightforward and highly producible synthesis of UV-resistant dendrimeric porous silica nanospheres (SiO_2−HBT) by adding benzotriazole as a pore-expanding agent, more importantly demonstrating its detailed mechanism. Well-dispersed silica nanospheres are shown to offer the release property for benzotriazole triggered by UV and heat irradiation while durable UV protection due to the supplementary of benzotriazole in the PBAT matrix. With benzotriazole compensation, the halving period of elongation at break performance was extended from about 15 to 48 h. Combined with gel content and gel permeation chromatography analyses, it was inferred that the process of crosslinking resulting from Norrish I can be effectively minimized by the action of SiO_2−HBT. The design of modified release strategy realizes the durable UV absorption ability of the hydroxyphenyl benzotriazole class of photostabilizers in particular but more generally highlights an important adding method that should be considered when utilizing a photostabilizer.
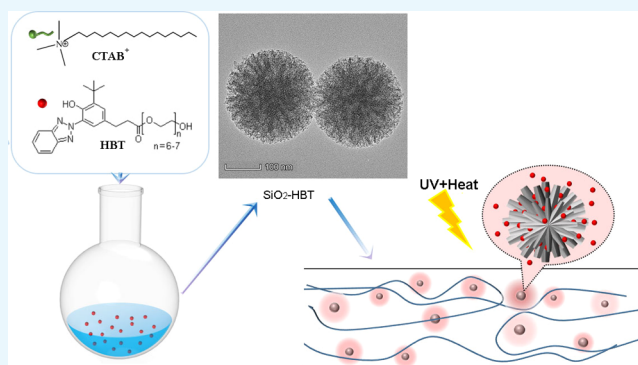
INTRODUCTION

Poly(butylene adipate-*co*-terephthalate) (PBAT) has been widely used in the biodegradable production of blown films and associated membrane products for high elongation at break, flexibility, and good processability suitable for several applications ranging from packaging materials to film cover crops.[1,2] However, PBAT is susceptible to ultraviolet (UV) radiation due to the presence of aromatic rings and carbonyl groups on its chain that act as photosensitizers.[3,4] Such UV aging would strongly influence the safety and service life of the corresponding products and thus limit the outdoor applications of PBAT materials.[5]

Normally, for the purpose of enhancing the weatherability and durability of PBAT and other polymers, UV absorbers, such as benzotriazole and triazine, are often used as UV light stabilizers, which are capable of absorbing UV photons and converting to nonradiative heat through excited-state intramolecular proton transfer (ESIPT).[6,7] The main disadvantages of UV absorbers with relatively low molecular weight are being easy to cause loss by migrating to the surface and volatilizing during heat processing, thus reducing its concentration and leading to the weakening of UV-resistant protection for polymer surface and film products. To overcome these drawbacks, there have been two widely explored ways. One is trending toward the increase in molecular weight and reactivity. Careful design and construction of molecular

structures can optimize the technical performance but not satisfy the economic performance, such as difficult implementation, increased cost, and unstability product performance, which limited a further commercialized promotion and application. The other is based on surface modification technologies, especially using blocking nanomaterials to enhance the thermostability and tolerance to migration to improve the UV-resistant property. Meanwhile, the modification with organic species can decrease considerably the nanomaterials' hydrophilicity and improve the interaction and compatibilization between the additive and polymer matrix, which favored the consequence of a better dispersion, distribution, and mechanical property in the polymer matrix. Due to the $\pi-\pi$ interactions between the phenyl rings and the aromatic rings of the polymeric chain, lignin[8] and phenybutyl isocyanate grafted on cellulose nanocrystals[9] can reinforce the mechanical properties of PBAT composites. It was also proved that both melanin-like polydopamine[10] and soda lignin grafted

by biobased oleic or undecylenic acids[11] are very promising tools to enhance the UV-blocking capability and photostability of PBAT films, while not negatively affecting the PBAT mechanical properties. According to these authors, the enhanced UV-resistant performance of modified composite nanomaterials is a result of multi-functionalization, good dispersion, and improved interfacial interaction due to surface modification.

Most authors prepared UV-resistant nanocomposites via chemically grafted functional groups on the surface of the nanomaterials. Undergoing a complex surface modification process without detriment to the intramolecular hydrogen bond is essential for the photostabilizing potential of these compounds. The total amount of modifiable UV absorbent is restricted by harsh reaction conditions and limited surface available modifiable groups, which is inevitably dependent on the dispersity and size of the nanocomposites. It is still challenging to simply make a robust PBAT nanocomposite film in combination with both excellent mechanical and UV-resistant performances. The development of a new approach to introduce an environmental friendly UV-resistant nano-composite, which can provide prolonged and even "smart" release of the stabilizing species on demand, becomes an important issue for many industries where an adequate UV protection is needed.

[3-[3-(2H-Benzotriazol-2-yl)-5-(1,1-dimethylethyl)-4-hydroxyphenyl]-1-oxopropyl]-hydroxypoly(oxo-1,2-ethanediyl) (HBT) is a commercially available o-hydroxyphenyl benzo-triazole class of photostabilizers for UV absorption covering both the UVA and UVB ranges. In order to provide adequate UV protection for PBAT films, we prepared a porous delivery system (SiO$_2$−HBT) via a dual-surfactant process (depicted in Scheme 1) without detriment to the chromophores of HBT. The release of HBT can be realized under the stimuli of external heat or UV irradiation, which indicates that more agents can be released due to this release mode, and finally, the UV absorber utilization rate in the anti-photo-aging system can be improved. A mesoporous silica skeleton is utilized to provide the thermostability and photostability, which are crucial for effective concentration in long-term protection.[12] Moreover, as a migration pathway, the open channel extends the migration route of HBT to realize the effective release concentration. The UV absorbance of SiO$_2$−HBT nanospheres was carefully investigated. The changes of mechanical and thermal properties of PBAT films with porous SiO$_2$−HBT under accelerated aging conditions were discussed in detail, and the UV-resistant mechanism of SiO$_2$−HBT can be further verified.

■ RESULTS AND DISCUSSION

Characterization of Porous SiO$_2$−HBT Nanospheres. Dendrimeric mesoporous silica nanospheres are self-assembly synthesized by a dual-surfactant assembly approach. The synthesis of SiO$_2$−HBT is presented in Scheme 1. Typically, the positively charged hexadecyltrimethylammonium bromide (CTAB) micelles act as the nucleation sites for the formation of microporous silica nanoparticles under alkaline conditions. Positive CTAB is also electrostatically bound to the negatively charged nanoparticle surface and facilitates the self-agglomer-ation of the nanoparticles into the larger spheres. Here, nonionic HBT was chosen as a cosurfactant to penetrate into parts of the hydrophobic core of the micelles formed by CTAB and thus increase its volume. The enlarged mesopore acts as

Scheme 1. Schematic Illustration of the Synthesis of Porous SiO$_2$−HBT Nanospheres in an Ethanol/Water Solution^a
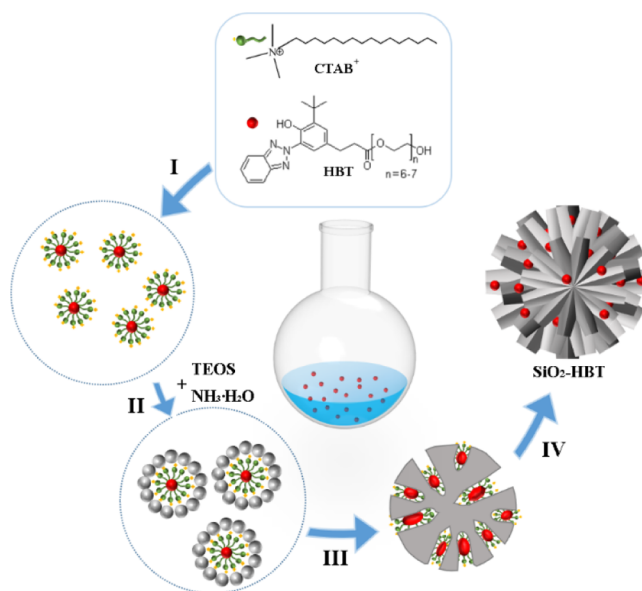

^{a}I: Formation of positive CTAB−HBT micelles (cationic cetyltri-methyl ammonium bromide (CTAB$^+$) surfactants and HBT as pore swelling agents), II: assembly of TEOS oligomers, III: the aggregate of silica radially from the center under steric-hindrance of enlarged CTAB micelles, and IV: the formation of dendrimeric mesoporous silica spheres (SiO$_2$−HBT).

the cargo agents to retain HBT inside. Meanwhile, enlarged CTAB micelles will act as a microtemplate with the steric hindrance effect endowing the aggregate of silica radially from the center and the formation of dendrimeric mesoporous silica spheres. Functionalization of the porous silica with hydrox-yphenyl triazole leads to enhancements of UV, especially UVA, absorbing abilities of the silica sphere and endows a low-polarity surface. Eventually, we got the porous silica hybrid nanocomposite whose surfaces and mesopores are embedded by hydroxyphenyl benzotriazole having the function of UV or heat responsiveness.

The morphology and porous structure of porous silica spheres can be proved by SEM and transmission electron microscopy (TEM). The SEM image (Figure 1A) shows that the obtained SiO$_2$−HBT samples were spherical, with an average diameter of ca. 250 nm and a clear pore structure. TEM characterization (Figure 1B) of porous silica spheres shows dendrimeric fibers arranged in three dimensions to form spheres with a perfect shape,[13] revealing radially growing branches, coming out from the center of the nanospheres, and distributed uniformly in all directions, giving the material an accessible porosity. These highly porous textures provided silica nanospheres more accessible interfaces to grip the polymer matrix fast. EDS mapping images of a single silica nanosphere (Figure 1C) validated the homogeneous distribu-tion of the nitrogenous specie on the surface of porous silica, which was evidenced to be from HBT and CTAB by X-ray photoelectron spectroscopy (XPS) analysis.

The mesoporous structure of SiO$_2$−HBT was further confirmed by N$_2$ physisorption (Figure 1D). It is found that the specific surface areas range from 220 to 426 m^2·g^{-1}. The increase of the specific surface area was mainly attributed to the increase of the micropores and mesopores in the materials.
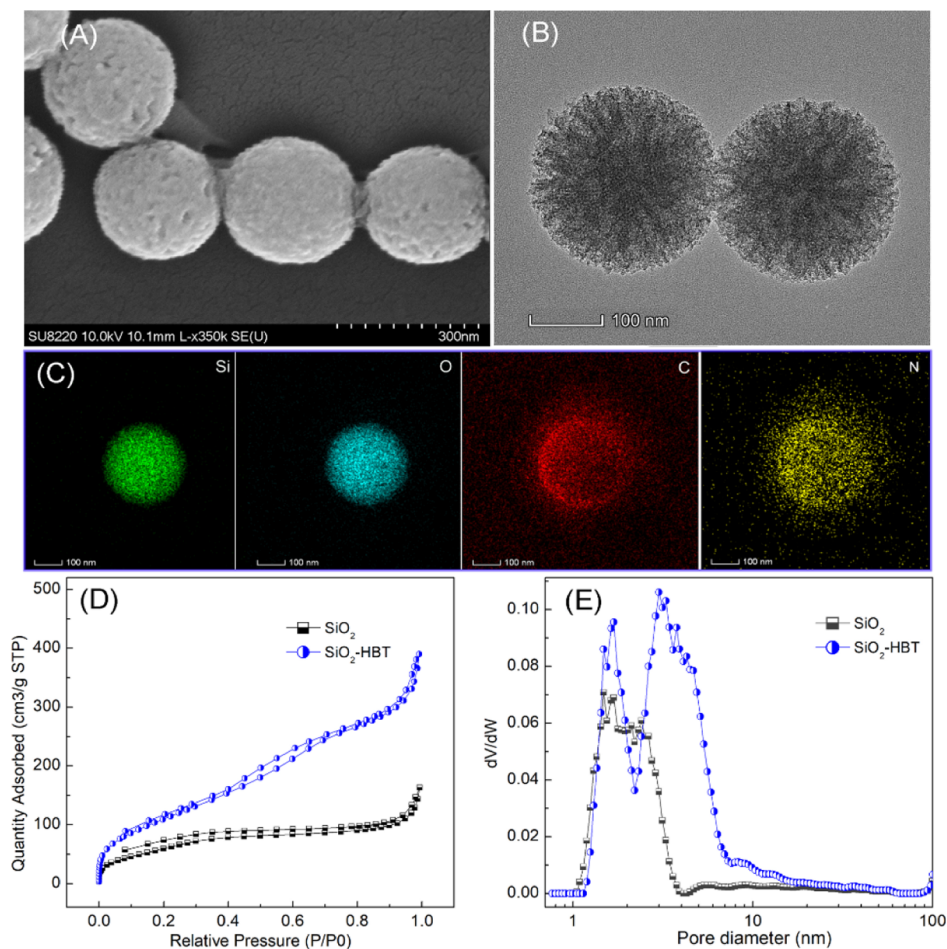
Figure 1. (A) SEM and (B) TEM images of SiO₂−HBT. (C) Elemental mapping images of SiO₂−HBT: Si, O, C, and N. (D) N₂ adsorption−desorption isotherms and (E) corresponding pore size distribution curves of SiO₂ and SiO₂−HBT.
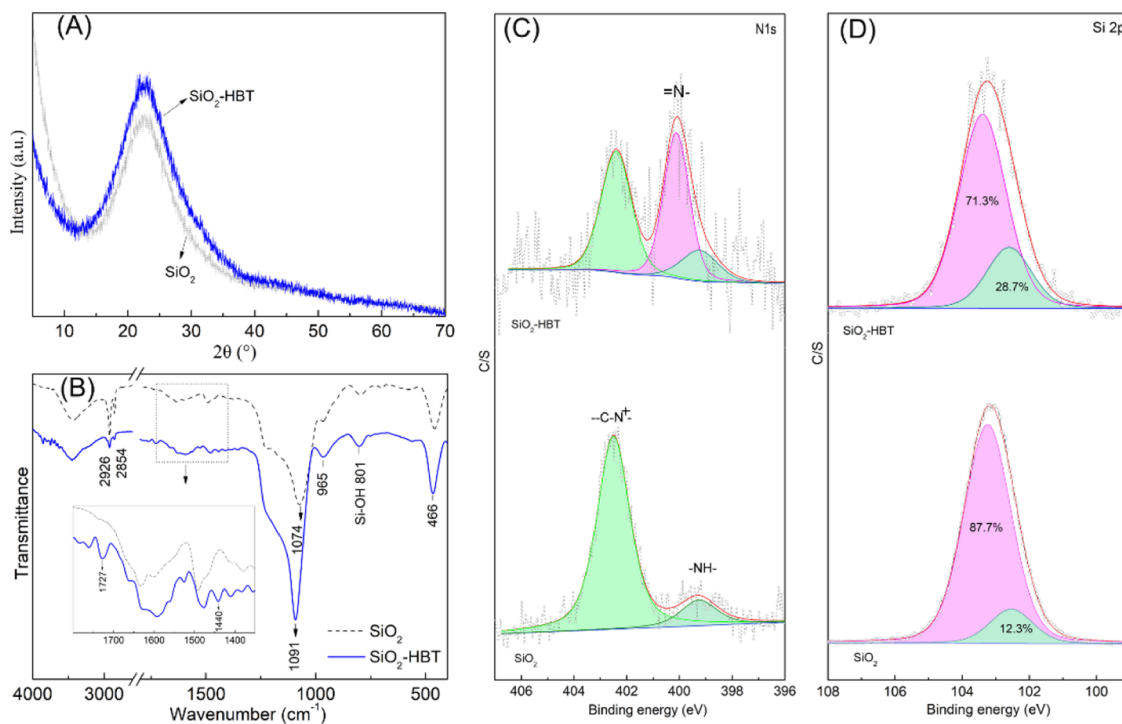
Figure 2. (A) XRD patterns, (B) FT-IR spectra, and high-resolution Si 2p (C) and N 1s (D) spectra of XPS of SiO₂ and SiO₂−HBT.

This was also reflected in the changes of the pore size distribution curves in Figure 1E. As shown, the pores in the materials are not monodisperse with a broader, asymmetric distribution. One can see that the pore diameter of silica increased from 1−4 to 1−8 nm with HBT as the pore-expanding agent. The average secondary pore size increases dramatically, yet without appreciable difference in primary pore size. The dramatic mesopore size enlargement confirms that HBT may penetrate into parts of the hydrophobic core of the micelles formed by CTAB and thus increase its volume. The large mesopores of ca. 10−30 nm observed by SEM and TEM images might only count for a small fraction of the total pore volume.[14]

The composition of the dendritic mesoporous hybrid spheres was confirmed by X-ray diffraction (XRD), Fourier transform infrared (FT-IR), and XPS analysis. The XRD patterns (Figure 2A) of the samples showed obvious broad peaks centered at 2θ of 23°, related to the amorphous scaffold of silica. The FT-IR spectrum (Figure 2B) of SiO_2 displays three characteristic peaks around 466, 801, and 1074 cm^{-1}, indicating the bending vibration, asymmetric stretching vibration, and anti-asymmetric stretching vibration of Si−O−Si in the silica skeleton. The bands at 2923 and 2852 cm^{-1} are attributable to the CH$_2$ symmetric and asymmetric stretching vibrations of the anchored CTAB backbone.[15] The characteristic peaks of CH$_2$ became weaker for SiO_2−HBT, accompanied by the new absorption peaks near 1440 and 1727 cm^{-1} arising from the benzene ring[16] and the stretching vibration mode of the carbonyl group in the ester bond of benzotriazole, respectively, indicating that benzotriazole was presented on the surface of SiO_2−HBT nanospheres. Meanwhile, a distinct up-shift of Si−O−Si from 1074 to 1091 cm^{-1} is observed after pore enlargement by HBT. This behavior has been observed previously and is related to the stoichiometry of SiO_x.[17] As more oxygen is incorporated into the sample, a more electronegative environment leads to shorter Si−O bond lengths and higher stretching frequencies.

The bonding configurations of nitrogen atoms in SiO_2 and SiO_2−HBT were characterized by high-resolution N 1s and Si 2p spectra (Figure 2C,D). It is known that the density of the electron cloud around the N atom decreases, the binding ability of the nucleus to the outside of the nucleus increases, and the binding energy (BE) of the N 1s orbital increases. The N 1s spectra fitted into three peaks at around 402.4, 400.0, and 399.2 eV are contributed to positively polarized nitrogen (−C−N$^+$−) atoms, imine nitrogen (=N−), and amine nitrogen (−NH−) group, respectively.[10] As shown by the N 1s spectra (Figure 2C), imine nitrogen (=N−) is the main component in the prepared SiO_2−HBT. In contrast, the imine nitrogen (=N−) fitting was silent for the pure SiO_2, clearly confirming that the benzotriazole functional groups were evenly modified on the silica skeleton, which was also evidenced by the element plane scan distribution in Figure 1C. The N contents on the surfaces of SiO_2−HBT and SiO_2 tested by XPS were 2.71 and 1.42%, respectively. The N content of the SiO_2−HBT composite can be further divided into 1.91% for CTAB and 0.8% for HBT. In addition, the high resolution of Si 2p spectra was consistent with two silica environments owing to BE at 103.2 and 102.6 eV, which was assigned to O−Si−O and −Si−O−C species (Figure 2D). Compared with pure SiO_2, it could be seen obviously that the peak area of Si−O−C increased after the pore-enlarged process with HBT, which indicated that the condensation of Si−O on

the surface layer is affected by HBT, and it was well in line with the result of the FT-IR spectrum. These facts further corroborated that part of HBT species had been bonded onto the exterior surface of SiO_2.[18]

Combining the above analysis results, we can confirm the successful modification of benzotriazole on the dendritic porous SiO_2−HBT nanospheres.

**Characterization of the SiO_2−HBT/PBAT Composite Film.** The UV absorption properties of the prepared SiO_2−HBT powder, the blank PBAT film, and the PBAT film with SiO_2−HBT were investigated by a UV−vis diffuse reflectance spectrophotometer in the wavelength range from 200 to 600 nm (Figure 3). The chromophore groups in aromatic polyesters such as PBAT absorb UV from 200 to 320 nm, which is likely to provoke photo-oxidation.
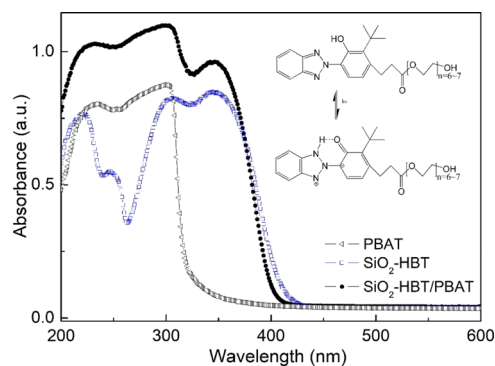
Figure 3. Absorption spectra of UV−vis spectroscopy from SiO_2−HBT powder, pure PBAT film, and PBAT composite film with 4 phr SiO_2−HBT. Inset is the ESIPT of the HBT molecule.

The absorption spectra of SiO_2−HBT nanospheres show a double-band structure in the long-wavelength UV region observed for most intramolecularly hydrogen-bridged UV absorbers. The shorter wavelength band at about 300 nm arises from a local transition within the benzotriazole moiety. The longer wavelength band at about 350 nm can be attributed to a $\pi-\pi^*$ charge-transfer state; this is favored by the planar orientation enforced by the intramolecular hydrogen bond. These spectral properties appear virtually unchanged in the spectra of the polymer matrix. Notably, it can be seen that the characteristic absorbance edge around 420 nm of SiO_2−HBT exhibits a hypochromatic shift effect in the PBAT matrix. As reported by Keck et al.,[7] the hypochromatic shift of the long-wavelength absorbance edge may be due to the formation of intermolecularly rather than intramolecularly hydrogen-bonded species. Dispersed in the PBAT matrix, a weak hydrogen-bonded interaction is expected to be formed between the hydroxyphenyl of HBT and the ester segment of the PBAT backbone, which leads to an increased activation barrier and to an enhanced minimum activation energy.

SEM micrographs of the surface and the fracture surface of the PBAT composite film with 4 phr SiO_2−HBT nanospheres are shown in Figure 4. The surface of the composite film is smooth, and the nanospheres are well dispersed in the fracture surface and grip the polymer matrix firmly. In addition to the weak hydrogen bond interaction discussed earlier, the compatibility for HBT was also dominated by the $\pi-\pi$ stacking interaction[19] between the aromatic ring of o-hydroxyphenyl triazole and the aromatic segment of the PBAT repeat unit. Silica nanoparticles remain adhered to the
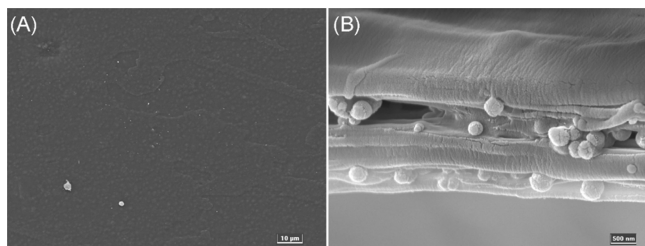
Figure 4. SEM micrographs of surface (A) and fracture surface (B) of the SiO_2−HBT/PBAT composite film.

fractured surface during the freeze-fracture process, which is direct evidence of the good adhesion between modified silica nanospheres and the PBAT matrix. It is known that the properties of the composite film strongly depend on the dispersion of the nanofillers in the polymeric matrix and the interaction between them. It is an effective method for increasing the compatibility and adhesion of nanocomposites and polymer films by generating the interaction and nanostructures at the interface.

Characterization of Durable UV Protection Property. The UV protection property of the PBAT nanocomposite film was evaluated by measuring the evolution of gel content, molecular weight, and mechanical properties during UV irradiation. The mechanical properties after UV irradiation directly reflect the UV-resistant capacity, which has a huge effect on the lifetime of materials. The retention rates of the elongation at break of PBAT films during the UV-accelerated aging process are depicted in Figure 5A. The elongations at break of both neat PBAT and SiO_2/PBAT films show a sharp decrease with the UV irradiation time. With two reverse compensation steps in the initial stage and the period of 18−24 h, the decrease of the SiO_2−HBT/PBAT film is decelerated from 91 to 57% after irradiation for 60 h. The mechanical properties demonstrate that the addition of SiO_2−HBT nanospheres can obviously improve the toughness of the films treated by UV irradiation.

Notably, the enhanced mechanical property of the SiO_2−HBT/PBAT film should be, at least partially, attributed to the HBT in the mesopore maturely triggered by external UV irradiation and high temperature during the service period. To further probe this hypothesis, ethanol was employed to investigate the release performance of SiO_2−HBT nanospheres. The spectra (Figure 5B) revealed that the release process was triggered by UVA and heat irradiation (40 °C),

while the pure magnetic stirring could not provide extra UV protection owing to the constant absorbance in the UV range. Indeed, the hydrogen bond system is thermodynamically unstable and can be easily constructed, resulting in a temperature-triggered benzotriazole component release. The dendrimeric porous structure does not completely inhibit the migration of benzotriazole but endows an effective addition and release to maintain the effective concentration in the matrix by UV/heat-responsive behaviors (Scheme 2), owing to the photochemical inertia property of silicon such as "safe house" and extended pathway. This simple UV/heat-responsive release system, free of initiators, provides a new platform for highly efficient release, which might hold promise in the applications of SiO_2−HBT as an outdoor product additive. Figure 5B clearly shows that the HBT concentration released from the SiO_2−HBT is remarkable and that the HBT amount in the modified nanospheres calculated from the concentration curve exceeds 66.7 mg·g^{-1}.

In order to survey UV protection, the evolution of the content of gels, the molecular weight, and the thermodynamic property were collected by Soxhlet extraction, gel permeation chromatography (GPC), and differential scanning calorimetry (DSC) analyses. Figure 6A shows the gel contents of an aged PBAT film and the SiO_2−HBT/PBAT composite film. As reported previously, the photodegradation produces both chain scission and crosslinking.[5,20] In the early stages of aging, the physical crosslinking produced by the radical prevails with a consequential decrease in elongation at break. In the presence of SiO_2−HBT, the photogenic crosslinking reaction time with 45% gel content yield is increased from 24 to 60 h. The reduction of gel content indicates that the crosslinking in the PBAT composite film is inhibited by SiO_2−HBT. Figure 6B shows the results of number-average molecular weight ($\overline{M_n}$) and dispersity for polymers ($\overline{M_w}/\overline{M_n}$) obtained by GPC analysis for the SiO_2−HBT/PBAT composite films before and after the UV-accelerated aging test. In our study, the values of $\overline{M_n}$ show a rise−fall change. In the early stage of aging (12−36 h), the higher $\overline{M_n}$ values, companied with the decreased dispersity between 1.49 and 1.70, presented a greater degree of crosslinking and/or branching in the portions of molecular weight of the distribution curve above 21.8 kg·mol^{-1}. Crosslinking in the PBAT matrix results from recombination of the generated free radicals from the reaction Norrish I and hydrogen abstraction, as previously reported by Kijchavengkul et al.[5] It is possible to infer that the crosslinking resulted from
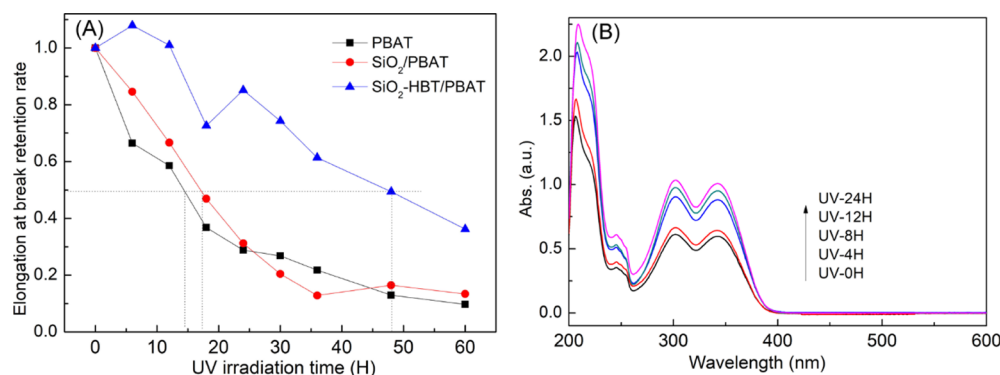
Figure 5. (A) Elongation at break retention rate of pure PBAT, SiO_2/PBAT, and SiO_2−HBT/PBAT films as a function of irradiation time. (B) UV−vis of SiO_2−HBT in ethanol solution as a function of UV irradiation time at 40 °C.

Scheme 2. Schematic Illustration of the Release Behavior of SiO₂−HBT Nanospheres in the PBAT Matrix Triggered by UV and Heat Irradiation
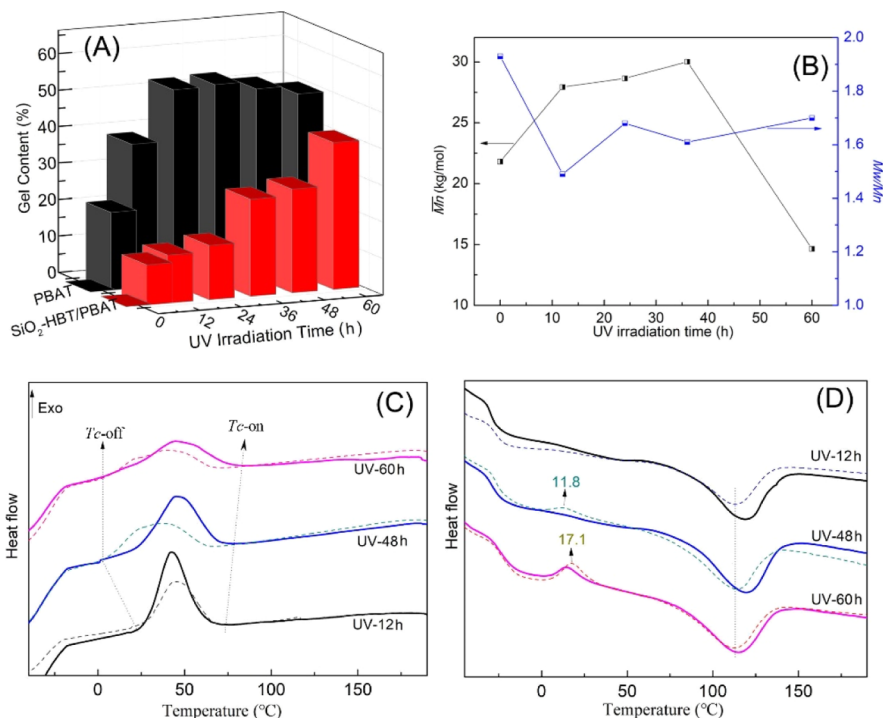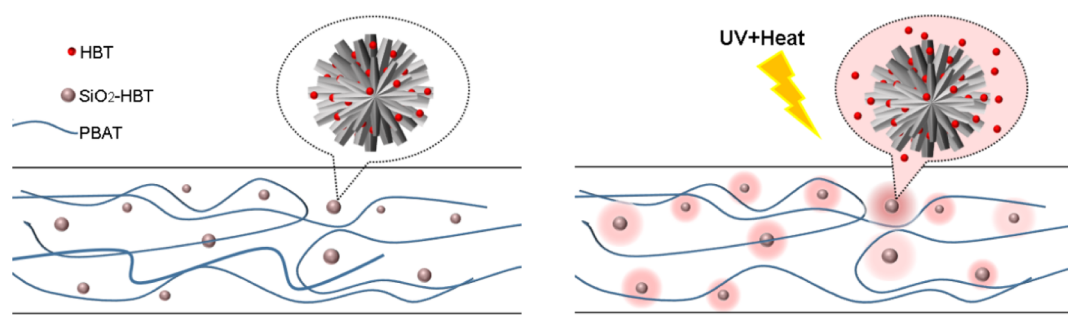
Figure 6. (A) Gel contents of pure PBAT and SiO₂−HBT/PBAT films as a function of irradiation time. (B) GPC traces of UV-exposed SiO₂−HBT/PBAT films: Dispersity for polymers $(\overline{M_w}/\overline{M_n})$ and number-average molecular weight $(\overline{M_n})$. (C) DSC cooling curves and (D) second heating curves of aged SiO₂−HBT/PBAT films (solid line —) and their corresponding gels (dash line ---), respectively.

Norrish I is minimized by the action of SiO₂−HBT. A decrease in the values of $\overline{M_n}$ was observed until the gel content reached a plateau stage, from which the chain scissions predominated. After 60 h of UV irradiation, the $\overline{M_n}$ values of the PBAT film and the SiO₂−HBT/PBAT composite film reduced to 9.1 kg· mol⁻¹ (initial 21.4 kg·mol⁻¹, reduced by 57.5%) and 14.6 kg· mol⁻¹ (initial 21.8 kg·mol⁻¹, reduced by 33.0%), respectively. According to the changes of the content of gel and molecular weight, the evolution of polymer structure during UV-accelerated aging can be roughly characterized. In the initial stage, the improved toughness is mainly due to the fact that a small increase in molecular weight results from longer polymer chains between the crosslink. With the increase of UV irradiation, the mechanical property deteriorated with the increased content of aged gels and low molecular weight oligomers. The composite SiO₂−HBT nanospheres can slow down the occurrence of crosslinking and chain scissions by absorbing UV rays during UV protection of the PBAT film.

DSC analysis of the aged film and the corresponding gels was used to further characterize and verify the crosslinking and chain scission. The exothermic peaks for aged SiO₂−HBT/ PBAT film crystallization process and their corresponding gels are shown in Figure 6C,D. The slight increase in T_g, the significant width in T_c, the appearance of cold crystallization peak (T_{cc}), and the slight decrease in the melting temperature (T_m) of SiO₂−HBT/PBAT films are highly consistent with the change of corresponding gels. The increase of T_c-on and T_c-peak is mainly attributed to chain scission, which leads to wider molecular weight distribution and wider crystallization temperature range. Moreover, it can be seen that the cold crystallization peaks (T_{cc}) of crosslinked gels become more obvious and shift from 11.8 to 17.1 °C with increasing aged time accompanied by the well-defined crystallization exothermic peaks (T_c) become wider. The poor cooling crystallization is attributed to the increased crosslinking degree and worse motility. The variation of thermodynamic property indicates that the unstable gels were constantly attacked by UV irradiation and undergo structural change. Considering gels

produced by the crosslinking reaction can greatly prolong the biodegradation cycle of the materials,[5] it is of great significance to avoid the generation of a crosslinked gel and slow down its further aging.

The thermal and mechanical results demonstrate that SiO_2–HBT nanospheres can be potentially used as a promising UV-resistant agent, so as to enhance the light stability and prolonged service lifetime of PBAT and related films.

◼ CONCLUSIONS

The dendrimeric porous silica nanospheres embedded with benzotriazole (SiO_2–HBT) were synthesized by a sol–gel method employing CTAB as a cationic surfactant and benzotriazole (HBT) as a pore-enlarging agent. The loaded benzotriazole group can facilitate porous silica a better UVA absorption performance by the intramolecular hydrogen bond and enhanced polymer compatibility by the hydrogen-bound reaction and π–π conjugation. The release of HBT triggered by UV and heat irradiation can maintain the concentration of small molecular UV absorber in the polymer matrix and effectively prolong the UV protection period. Addition with 4 phr SiO_2–HBT nanospheres, the photogenic crosslink reaction time with 45% gel content yield is prolonged from 24 to 60 h. After 60 h of UV irradiation, the reduction rate of number-average molecular weight ($\overline{M_n}$) of soluble part in hexafluoroisopropanol is decreased from 57.5 to 33.0%. Benzotriazole-modified porous silica is benefited for maintaining toughness under the UV rays and elongating the lifetime of PBAT materials, where the crosslink and chain scission are evidently decreased. We believe that this work demonstrates that modified porous release strategy can be used to develop a highly efficient photostabilizer.

◼ EXPERIMENTAL SECTION

Materials. HBT was purchased from Macklin (Shanghai Macklin Biochemical Co., Ltd.). PBAT was used as a polymer matrix, which receives the commercial name of Ecoflex C1200 (BASF, Germany). CTAB (98%), ammonia aqueous solution (28%), tetraethyl orthosilicate (TEOS), dichloromethane (DCM), and the other reagents were purchased from Sigma-Aldrich and used as received.

Preparation of Porous SiO_2–HBT Nanospheres. Porous silicon nanospheres embedded with HBT were fabricated using a simple procedure at room temperature. In a single-neck flask, 0.9 g of CTAB was first dissolved into 50 mL of deionized water. Second, 1.5 mL of HBT mixed with 200 mL of ethanol solution was added and ultrasounded for half an hour to form an even white emulsion. Then, 12 mL of TEOS and 2 mL of ammonia aqueous solution were also dripped into the above system and stirred for another 3 h. The resultant product was collected by suction filtration using the Büchner funnel and washed to neutral with deionized water. Finally, the collected white powder (SiO_2–HBT) was lyophilized overnight and dried at 80 °C for 24 h to remove moisture. The preparation process of SiO_2 was the same as described above, except that no light stabilizer HBT was added.

Preparation of the SiO_2–HBT/PBAT Composite Film. In our study, PBAT was used as a polymer source to form a composite film through solvent casting. The DCM solution of PBAT containing 4 phr (parts per hundred parts of PBAT) SiO_2–HBT was placed on the glass plate, scraped flat, and

dried in fume hood. The thickness of the SiO_2–HBT/PBAT composite film was controlled at 25 ± 1 μm. The films were cut into 1 cm wide strips before accelerated aging test and mechanical property test.

UV-Accelerated Aging. The UV aging experiment was carried out in a QUV-accelerated weathering tester (Q-Lab Co. Ltd.) with a UVA-340 lamp in the condition of 0.89 W/m^2 at 50 °C. The films were tested every 6 or 12 h until 60 h.

The gel contents of the composite films were measured by Soxhlet extraction using DCM as the solvent. The extracting solution was dried at 50 °C for GPC tests. The gel content X_g was calculated using equation

$$ X_g \% = \left(1 - \frac{M_0 - M_1}{M} \right) \times 100 $$

where M_0 is the total weight of the film and filters, M_1 is the residual weight of the film and filters after 24 h of extraction, and M is the initial weight of the film.

Simulant for Release Study. An independent release study was conducted an alcohol system at 40 °C because HBT has very low water solubility. SiO_2–HBT (5 mg) mixed with 50 mL of ethanol solution was sealed in a quartz tube.

Characterization. The morphologies of the nanospheres and coatings were studied using a JEOL SU8220. TEM was carried out (FEI Talos F200s). STEM–EDS spectra were recorded from a Talos 200s instrument operated at 200 kV. XRD was used to determine the crystallographic phase of SiO_2 and SiO_2–HBT on a Rigaku D/2 MAX-2500 diffractometer using Cu Kα radiation. The N$_2$ sorption isotherms were measured at 77 K (Micromeritics ASAP 2460.3.01). Before measurement, the samples were degassed in a vacuum at 120 °C for 12 h. The surface areas were calculated by the Brunauer–Emmett–Teller method using the adsorption data in a relative pressure (P/P_0) range from 0.005 to 0.25. By using the Barrett–Joyner–Halenda method, the pore size distribution and pore volume were calculated out from the adsorption branches of isotherms. FT-IR spectra were recorded on a Bruker Vector 33 FT-IR spectrometer (KBr disk). UV–vis transmission spectra were recorded on a Shimadzu UV-2600 spectrophotometer with a bandwidth of 2 nm, a medium scanning rate, and quartz cuvettes of 1 cm path length. The chemical surface analysis was performed by XPS using a conventional XPS spectrometer (Thermo Fisher Scientific K-Alpha+) with a stationary analyzer with monochromatic Al Kα X-ray radiation as the excitation source. The BE was calibrated to surface contamination C 1s (284.8 eV). The composition of Si 2p and N 1s spectra was acquired according to the Gaussian fitting. To study the effect of UV irradiation on the elongation at break of PBAT films, tensile test on five samples for each aged mulch film was conducted using an MTS Exceed model E43 mechanical testing machine in accordance with the standard ASTM D882 method. The number-average molecular weight ($\overline{M_n}$), weight-average molecular weight ($\overline{M_w}$), and its distribution ($\overline{M_w}/\overline{M_n}$) of extractive were investigated by GPC (PL-GPC50, Agilent) using hexafluoroisopropanol as the mobile phase. The DSC study performed using a Discovery DSC 25 (TG, America). The samples were heated up to 190 °C at a heating rate of 20 °C·min^{-1} under a nitrogen atmosphere and held at that temperature for 1 min in order to erase any thermal history. Then, the samples were cooled to −50 °C at a cooling rate of 20 °C·min^{-1} and then re-heated again up to 190 °C at a heating rate of 10 °C·min^{-1}. From this

second DSC scan, the glass-transition temperature (T_g) or the melting point (T_m) of the samples was recorded.

■ AUTHOR INFORMATION

Corresponding Authors

Xiaoyan Sun − Institute of Biological and Medical Engineering, Guangdong Academy of Sciences, Guangzhou 510316, China; Guangdong Biomaterials Engineering Technology Research Center, Guangzhou 510316, China; ● orcid.org/0000-0002-1718-5430; Email: xy_s200906@163.com

Dong Xie − Institute of Biological and Medical Engineering, Guangdong Academy of Sciences, Guangzhou 510316, China; Guangdong Biomaterials Engineering Technology Research Center, Guangzhou 510316, China; Email: xd0929@163.com

Authors

Ke Wang − Institute of Biological and Medical Engineering, Guangdong Academy of Sciences, Guangzhou 510316, China; Guangdong Biomaterials Engineering Technology Research Center, Guangzhou 510316, China; ● orcid.org/0000-0002-6163-4512

Hailu Liu − Institute of Biological and Medical Engineering, Guangdong Academy of Sciences, Guangzhou 510316, China; Guangdong Biomaterials Engineering Technology Research Center, Guangzhou 510316, China

Yang Zhao − Institute of Biological and Medical Engineering, Guangdong Academy of Sciences, Guangzhou 510316, China; Guangdong Biomaterials Engineering Technology Research Center, Guangzhou 510316, China

Yuan Li − Institute of Biological and Medical Engineering, Guangdong Academy of Sciences, Guangzhou 510316, China; Guangdong Biomaterials Engineering Technology Research Center, Guangzhou 510316, China

Complete contact information is available at:
https://pubs.acs.org/10.1021/acsomega.1c05682

Notes

The authors declare no competing financial interest.

■ REFERENCES

(1) Ghosh, K.; Jones, B. H. Roadmap to biodegradable plastics-current state and research needs. ACS Sustainable Chem. Eng. 2021, 9, 6170−6187.

(2) Khan, H.; Kaur, S.; Baldwin, T. C.; Radecka, I.; Jiang, G.; Bretz, I.; Duale, K.; Adamus, G.; Kowalczuk, M. Effective control against broadleaf weed species provided by biodegradable PBAT/PLA mulch film embedded with the herbicide 2-methyl-4-chlorophenoxyacetic acid (MCPA). ACS Sustainable Chem. Eng. 2020, 8, 5360−5370.

(3) De Hoe, G. X.; Zumstein, M. T.; Getzinger, G. J.; Rüegsegger, I.; Kohler, H.-P. E.; Maurer-Jones, M. A.; Sander, M.; Hillmyer, M. A.; McNeill, K. Photochemical transformation of poly(butylene adipate-co-terephthalate) and its effects on enzymatic hydrolyzability. Environ. Sci. Technol. 2019, 53, 2472−2481.

(4) Maurer-Jones, M. A.; Monzo, E. M. Quantifying photochemical transformations of poly(butylene adipate-co-terephthalate) films. ACS Appl. Polym. Mater. 2021, 3, 1003−1011.

(5) Kijchavengkul, T.; Auras, R.; Rubino, M.; Alvarado, E.; Montero, J. R. C.; Rosales, J. M. Atmospheric and soil degradation of aliphaticearomatic polyester films. Polym. Degrad. Stab. 2010, 95, 99−107.

(6) Tobita, S.; Yamamoto, M.; Kurahayashi, N.; Tsukagoshi, R.; Nakamura, Y.; Shizuka, H. Effects of electronic structures on the excited-state intramolecular proton transfer of 1-hydroxy-2-aceto-naphthone and related compounds. J. Phys. Chem. A 1998, 102, 5206−5214.

(7) Keck, J.; Kramer, H. E. A.; Port, H.; Hirsch, T.; Fischer, P.; Rytz, G. Investigations on polymeric and monomeric intramolecularly hydrogen-bridged UV absorbers of the benzotriazole and triazine class. J. Phys. Chem. 1996, 100, 14468−14475.

(8) Zhang, Y.; Naebe, M. Lignin: A review on structure, properties, and applications as a light-colored UV absorber. ACS Sustainable Chem. Eng. 2021, 9, 1427−1442.

(9) Morelli, C. L.; Belgacem, M. N.; Branciforti, M. C.; Bretas, R. E. S.; Crisci, A.; Bras, J. Supramolecular aromatic interactions to enhance biodegradable film properties through incorporation of functionalized cellulose nanocrystals. Composites, Part A 2016, 83, 80−88.

(10) Xing, Q.; Buono, P.; Ruch, D.; Dubois, P.; Wu, L.; Wang, W.-J. Biodegradable UV-blocking films through core-shell lignin-melanin nanoparticles in poly(butylene adipate-co-terephthalate). ACS Sustainable Chem. Eng. 2019, 7, 4147−4157.

(11) Xing, Q.; Ruch, D.; Dubois, P.; Wu, L.; Wang, W.-J. Biodegradable and high-performance poly(butylene adipate-co-terephthalate)-lignin UV-blocking films. ACS Sustainable Chem. Eng. 2017, 5, 10342−10351.

(12) Knežević, N. Ž.; Ilić, N.; Đokić, V.; Petrović, R.; Janaćković, Đ. Mesoporous silica and organosilica nanomaterials as UV-blocking agents. ACS Appl. Mater. Interfaces 2018, 10, 20231−20236.

(13) Cecílio, D. M.; Fernandes, A.; Lourenço, J. P.; McKenna, T. F. L.; Ribeiro, M. R. Innovative route for the preparation of high-performance polyolefin materials based on unique dendrimeric silica particles. Polym. Chem. 2021, 12, 4546−4556.

(14) Du, X.; He, J. Fine-tuning of silica nanosphere structure by simple regulation of the volume ratio of cosolvents. Langmuir 2010, 26, 10057−10062.

(15) Seentrakoon, B.; Junhasavasdikul, B.; Chavasiri, W. Enhanced UV-protection and antibacterial properties of natural rubber/rutile-TiO2 nanocomposites. Polym. Degrad. Stab. 2013, 98, 566−578.

(16) Liao, T.; Liu, C.; Ren, J.; Chen, H.; Kuang, Y.; Jiang, B.; Chen, J.; Sun, Z.; Li, C. A chitosan/mesoporous silica nanoparticle-based anticancer drug delivery system with a "tumor-triggered targeting" property. Int. J. Biol. Macromol. 2021, 183, 2017−2029.

(17) DuMont, J. W.; Marquardt, A. E.; Cano, A. M.; George, S. M. Thermal atomic layer etching of SiO2 by a "conversion-etch" mechanism using sequential reactions of trimethylaluminum and hydrogen fluoride. ACS Appl. Mater. Interfaces 2017, 9, 10296−10307.

(18) Wang, H.; Fu, Z.; Zhao, X.; Li, Y.; Li, J. Reactive nanoparticles compatibilized immiscible polymer blends: synthesis of reactive SiO2 with long poly(methyl methacrylate) chains and the in situ formation of Janus SiO2 nanoparticles anchored exclusively at the interface. ACS Appl. Mater. Interfaces 2017, 9, 14358−14370.

(19) Xu, J.; Xu, F.; Qian, M.; Xu, F.; Hong, Z.; Huang, F. Conductive carbon nitride for excellent energy storage. Adv. Mater. 2017, 29, 1701674.

(20) Malanowski, P.; van Benthem, R. A. T. M.; van der Ven, L. G. J.; Laven, J.; Kisin, S.; de With, G. Photo-degradation of poly-(neopentyl isophthalate). Part II: Mechanism of cross-linking. Polym. Degrad. Stab. 2011, 96, 1141−1148.